European Radiology (2019) 29:4730–4741
https://doi.org/10.1007/s00330-019-06017-x

ONCOLOGY

Imaging features of SMARCA4-deficient thoracic sarcomas: a multi-centric study of 21 patients

Amandine Crombé[1,2] · Nicolas Alberti[1] · Nicolas Villard[3] · Frank Pilleul[3] · Xavier Buy[1] · François Le Loarer[2,4] · Michèle Kind[1]

Received: 3 September 2018 / Revised: 15 December 2018 / Accepted: 17 January 2019 / Published online: 14 February 2019

Abstract

Objectives *SMARCA4*-deficient thoracic sarcoma (SMARCA4-DTS) is a recently identified aggressive subtype of sarcoma. The aim of this study was to characterize the CT imaging features of SMARCA4-DTS.

Methods From June 2011 to May 2017, 21 adult patients with histologically proven SMARCA4-DTS were identified in the radiological database of 2 French sarcoma reference centers with at least one chest CT scan available. The locations, sizes, heterogeneity, margin definitions, and local extensions of the tumors were reported together with their impact on surrounding organs and regional and distant metastases. Pathological findings, molecular analyses, and patients' outcomes were retrieved.

Results Of the 21 included patients (median age 48, range 30–74), 18 (85.7%) were male and 18 (85.7%) had a smoking history. Four main radiological patterns were identified depending on the location of the main tumor burden: mediastinal ($n = 13$), pleural ($n = 6$), cervical ($n = 1$), and retroperitoneal ($n = 1$). Median size was 120 mm (range 46–266). Characteristic CT imaging features of primary tumors included ill-defined margins ($n = 21$), heterogeneous enhancement after injection ($n = 20$), multi-compartment extension from mediastinum to lung apex, pleura, or neck ($n = 20$), compressive effect responsible for atelectasis ($n = 11$), vascular encasement ($n = 16$—5 superior vena cava syndrome), and esophagus invasion ($n = 5$). Primary tumors showed strong ^{18}F-FDG avidity in eight patients with PET-CT. Necrotic lymphadenopathies were found in 19 patients, with a surrounding infiltrate in 13 patients. Metastatic locations at baseline mainly involved adrenal ($n = 10$), lung ($n = 6$), and bone ($n = 5$). Median overall survival was 5 months (range 1–13).

Conclusion Most SMARCA4-DTS present with compressive and infiltrative chest masses with ill-defined necrotic lymphadenopathies. The diagnosis of SMARCA4-DTS should enter in the differentials of the radiologist, especially in the case of a rapidly evolving thoracic mass in young smoking males.

Key Points

- *SMARCA4-DTS is a very aggressive poorly differentiated sarcoma with a predilection for young and middle-aged adult male smokers.*
- *SMARCA4-DTS, which is mostly located in the chest cavity, can compress and infiltrate all adjacent organs leading to superior vena syndrome, lung atelectasis, epiduritis, spinal cord compression, and esophagus invasion.*
- *SMARCA4-DTS typically demonstrates several ill-defined necrotic lymphadenopathies spreading in axillar, subclavian, cervical, mediastinum, and retroperitoneum.*

François Le Loarer and Michèle Kind codirected the research.

Electronic supplementary material The online version of this article (https://doi.org/10.1007/s00330-019-06017-x) contains supplementary material, which is available to authorized users.

✉ Amandine Crombé
a.crombe@bordeaux.unicancer.fr

[1] Department of Radiology, Institut Bergonié, Comprehensive Cancer Center, 229, cours de l'Argonne, F-33000 Bordeaux, France

[2] University of Bordeaux, F-33000 Bordeaux, France

[3] Department of Radiology, Centre Léon Bérard, Comprehensive Cancer Center, F-69000 Lyon, France

[4] Department of Pathology, Institut Bergonié, Comprehensive Cancer Center, F-33000 Bordeaux, France

Keywords Sarcoma · Tomography, emission-computed · Lung neoplasms · Lymphoma

Abbreviations

^{18}F-FDG-PET/CT	^{18}F-Fluorodeoxyglucose positron emission tomography merged with computed tomography
BRG1	Brahma-related gene 1
HES	Hematoxylin and eosin staining
IASLC	International Association for the Study of Lung Cancer
MNSGCT	Malignant non-seminomatous germ cell tumor
MRT	Malignant rhabdoid tumors
NMC	NUT (*nuclear in testis*) midline carcinoma
NSCLC	Non-small cell lung carcinoma
NUT	Nuclear in testis
SCLC	Small cell lung carcinoma
SFT	Solitary fibrous tumor
SMARCA4-DTS	*SMARCA4*-deficient thoracic sarcoma
SOX2	Sex-determining region Y-bOX 2
SUVmax	Maximal standardized uptake value
TTF1	Thyroid transcription factor 1

Introduction

SMARCA4-deficient thoracic sarcomas (SMARCA4-DTS) are a recently identified subtype of sarcoma. They are characterized by inactivating mutations of SMARC4, which they share with malignant rhabdoid tumors (MRT) [1]. Although MRT affect the pediatric population, they are biologically close to SMARCA4-DTS since both tumor types display similar expression profiles and aggressive clinical courses (SMARCA4 encodes for BRG1 (Brahma-related gene 1), which is a key subunit of a chromatin remodeling complex that regulates transcription activity in cells) [2–4]. Even if only three studies have been conducted yet, there are striking similarities among the cohorts: these tumors are most often found in the chest of young and middle-aged males with a smoking history and show a rapid and unfavorable course with an overall survival of less than 8 months [1, 5, 6]. Patients typically demonstrate a compressive and infiltrative mediastinal mass responsible for superior vena cava syndrome. This initial presentation explains that the first suspected diagnosis is often a lymphoma. However, when addressed to a comprehensive cancer center, the alternate diagnostic hypothesis can also be a NUT (nuclear in testis) midline carcinoma (NMC), a recent entity with an aggressive course that can also be found in young adults [7–9].

There is an expanding literature about the pathological characterization of SMARCA4-DTS, but the details of their radiological aspects have not been described yet. Due to the rapidly evolving and aggressive course of the tumors, radiologists could play an important role if radiological features reminiscent of the diagnosis were identified. Radiologists could help guide immunohistochemistry and molecular analyses to perform on limited biopsy samples [10]. Indeed, Le Loarer et al have identified potential immunohistochemistry surrogate markers of SMARCA4-DTS that are not systematically performed when screening a thoracic mass [1]. Moreover, despite their very aggressive behavior, the lack of guidelines, and the inefficiency of classical chemotherapies, tailored therapies could already be available against SMARCA4-DTS [11–13]. Tazemetostat, an inhibitor of Enhancer of Zeste Homologue 2 (which is an histone lysine methyltransferase), has demonstrated a positive anti-tumor effect against SMARCA4-deficient solid tumors in a phase 1 study, and 4 clinical trials are currently opened for these patients [13] (https://clinicaltrials.gov).

Therefore, our aim was to describe the CT imaging features of these tumors at a local level through a pattern-based approach but also of their metastatic spreading and to discuss their differential diagnoses. To do so, we retrospectively analyzed the pre-treatment imaging of a case series of 21 patients with histologically proven SMARCA4-DTS from 2 sarcoma reference centers between June 2011 and May 2017.

Materials and methods

Patients

Patients were identified through the pathological database and the PACS system of 2 French sarcoma reference centers (Centre Léon Bérard in Lyon and Institut Bergonié in Bordeaux). We retrieved 45 patients with a pathological diagnosis of SMARCA4-DTS. Twenty-one patients were included as they presented with a baseline CT examination performed between June 2011 and May 2011. Of them, 11 were previously reported in a non-radiological study [1]. Twenty-four were excluded for lack of in-house baseline imaging data.

The following information was retrieved from the medical record: age, gender, medical history, smoking history and/or cannabis consumption, initial clinical symptoms, first suspected diagnosis by the radiologist and the pathologist, treatment, and outcome. This multi-center retrospective study was approved by the institutional review boards.

Imaging acquisitions

All patients had a baseline CT examination available, which was carried out on different scanners as the series included patients secondarily referred to our institution (32 to 64 multi-detector row CT scans, range of slice thickness 1.25–3 mm, axial plane of reformatting available in all cases). One patient had a chest CT without contrast agent administration alone. Twenty patients had a chest CT with contrast agent injection. Sixteen patients had an additional acquisition on the abdomen and pelvis with a contrast agent injection. Five patients had an acquisition on the brain because of neurologic symptoms (1 MRI and 4 CTs with contrast agent injection). Eight had a whole-body ^{18}F fluorodeoxyglucose positron emission tomography (^{18}F-FDG-PET/CT) performed on different systems from comprehensive cancer centers and following the European Organization for Research and Treatment of Cancer recommendations [14].

Imaging analysis

Two board-certified radiologists, including one senior radiologist from a French sarcoma reference center, independently reviewed the whole imaging dataset (inter-observer agreements are given in Supplementary Table 1). Secondly, they performed another reading of all the CTs together in consensus, which was based on the statistical analysis. They reported the following features: measure of the longest diameter (in mm); main radiological pattern among mediastinal, pleural, cervical, or abdominal (depending on the primary tumor location or the location of the dominant lesion burden when other anatomical locations were involved by the tumor); multicompartmental lesions when at least two of the radiological patterns were combined; heterogeneity after iodine-contrast agent administration (defined as the percentage of tumor volume with presence of low attenuations, iso- and high attenuations compared to muscle and categorized as homogeneous, $< 50\%$ heterogeneous, $\geq 50\%$ heterogeneous); presence of cystic component (defined as well-defined area with fluid-like attenuation and no enhancement after contrast agent injection); presence of calcification; presence of an abnormal tumor vascularization; margin definition of the main tumor component (categorized as well-defined, ill-defined on $<$ 25% of tumor circumference, ill-defined on $\geq 25\%$ of tumor circumference). When ^{18}F-FDG-PET/CT was performed, the maximal standardized uptake value (SUVmax) of the whole tumor burden was calculated.

Regarding the mediastinal lesions, the radiologists reported the following features: measure of the longest diameter, extension in craniocaudal axis and anteroposterior axis (upper/middle/lower mediastinum and anterior/posterior mediastinum, respectively), presence of a pericardial effusion, presence of thymus or esophagus invasion (defined as tumor budding within the mucosa) or lung apex extension, presence of a vascular encasement (none, hilar, superior vena cava syndrome, other vessels among the axillar, innominate, subclavian, and jugular veins), and presence of a post-obstructive lung atelectasis.

Regarding the pleural lesions, the following items were reported: measure of the longest diameter, uni- or bilateral location when present, and presence of a pleural effusion.

Lymph node metastases were defined as lymph nodes with a small diameter above 10 mm, without central fat, with an avidity on ^{18}F-FDG-PET/CT (when available), and showing alterations on the following CT scans. Lymph node metastases were evaluated as follows: areas (categorized as pulmonary-mediastinal [i.e., 2R/L, 3R/L, 4R/L, 5R/L, 6R/L, 7R/L, 8 R/L, 9R/L, 10R/L, 11R/L] according to the International Association for the Study of Lung Cancer [IASLC] lymph node map); internal thoracic, cervical-subclavian (i.e., 1R/L according to the IASLC lymph node map and/or located in any other lymph node of the cervix); axillary or abdominal (intra- or retroperitoneal); number of lymph node areas (0, 1, 2–5, > 5); presence of necrotic lymphadenopathy; and presence of a surrounding infiltrate. The presence of metastases was also reported (adrenal, liver, lung, bone, spleen, epidural, intra- or retroperitoneal sarcomatosis). Metastases were defined as abnormal solid lesions with avidity on ^{18}F-FDG-PET/CT (when available), which were not compatible with benign lesions and that showed changes in size and architecture on the following CT scans.

Pathological analysis

An expert pathologist reviewed all the cases in this study. All pathological specimens were assessed with hematoxylin and eosin staining (HES). Immunohistochemistry panels were completed with the surrogate markers of SMARCA4-DTS, using CD34, SOX2 (sex-determining region Y-bOX 2), and SMARCA4 (BRG1) (in 21, 19, and 21 patients, respectively); with NMC markers (NUT staining in 10 patients); with carcinoma markers (thyroid transcription factor 1 (TTF1) staining in 18 patients, keratin expression AE1/AE3 in 16 patients, p40/p63 in 14 patients); with thymic carcinoma markers (CD117/CD5 expression in 16 patients); and with neuroendocrine markers (chromogranin A and synaptophysin expressions in 11 patients). RNA sequencing to assess the SMARCA4 mutational status was screened in 12 patients.

Statistical analysis

Classical descriptive statistics were calculated. Numeric variables were expressed as mean ± standard deviation and/or median and range, as appropriate. Ordinal and categorical variables were given with the number of patients and

Table 1 Patient characteristics and presenting symptoms

Characteristics	No. of patients (%)
Age (years)	48 (30–74)
< 30	0/21 (0%)
30–50	11/21 (52.4%)
> 50	10/21 (47.6%)
Gender	
Male	18/21 (85.7%)
Female	3/21 (14.3%)
Tobacco history	18/21 (85.7%)
Cannabis intoxication	4/21 (19%)
Lung emphysema	11/21 (52.4%)
Presenting symptoms	
Dyspnea	11/21 (52.4%)
Chest pain	9/21 (42.9%)
Superior vena cava syndrome	5/21 (23.8%)
Pancoast-Tobias syndrome	2/21 (9.5%)
Epigastralgia	2/21 (9.5%)
High digestive hemorrhage	2/21 (9.5%)
Hemoptysis	1/21 (4.8%)

Age is given as median and range. Results are number (no.) of patients/total number of patients with available information and percentage in parentheses

percentages. Statistical analyses were performed using the SPSS statistical package (version 21.0, IBM).

Results

Clinical features

Clinical features are summarized in Table 1. Mean age was 48.1 ± 14.5 years old (range 30–74). There was a marked male predominance and most patients had a smoking history. Of the 18 patients with a smoking history, the consumption was quantified in 15 patients providing a median of 20 pack-years (range 6–20). Two patients quit before the diagnosis of SMARCA4-DTS: 1 year before after a 17-pack-year consumption and 15 years before after a 15-pack-year consumption. The most frequent clinical presentation was dyspnea (11 patients). Indirect symptoms of regional invasion were frequently observed during the first medical consultation: five patients had a superior vena cava syndrome, two had Pancoast-Tobias syndrome, two had high digestive hemorrhages, and one had hemoptysis.

Radiological presentation

Table 2 summarizes the radiological features seen on the first CT examination, prior to any treatment. We identified four main radiological patterns: mediastinal in 13 patients (61.9%), pleural in six patients (28.6%), cervical in one patient (4.8%), and retroperitoneal in one patient (1%) (Fig. 1). Almost all patients demonstrated a multi-compartment infiltrative and compressive extension, mostly mediastinal and unilateral pleural with thoracic and cervical lymphadenopathies. The tumor displayed a

Table 2 Imaging features of patients with *SMARCA4*-deficient thoracic sarcoma on initial chest CT

Characteristics	No. of patients (%)
2.a. Main pattern	
Mediastinal	13/21 (61.9%)
Pleural	6/21 (28.6%)
Cervical	1/21 (4.8%)
Retroperitoneal	1/21 (4.8%)
Multi-compartment extension	19/21 (90.5%)
Longest diameter (mm)	128 ± 57 (46–266)
Heterogeneity after injection	
Homogeneous	0/20 (0%)
< 50% heterogeneity	14/20 (70%)
≥ 50% heterogeneity	6/20 (30%)
Calcification	0/21 (0%)
Cystic component	0/21 (0%)
Margin definition	
Well-defined	0/21 (0%)
< 25% ill-defined	2/21 (9.6%)
≥ 25% ill-defined	19/21 (90.5%)
Abnormal vascularization	1/20 (5%)
18-FDG-PET-CT ($n = 8$)	
SUVmax	16.6 ± 8.2 (9.1–33.8)
2.b. Mediastinal component	
Longest diameter (mm)	127.6 ± 56.6 (46–266)
Craniocaudal	
Upper mediastinum	18/21 (85.7%)
Middle mediastinum	19/21 (90.5%)
Lower mediastinum	7/21 (33.3%)
Anteroposterior	
Anterior mediastinum	17/21 (81%)
Posterior mediastinum	16/21 (76.2%)
Pericardial effusion	6/21 (28.6%)
Thymus invasion	10/21 (47.6%)
Lung apex extension	14/21 (66.7%)
Post-obstructive atelectasis	11/21 (52.4%)
Esophagus invasion	
No	8/21 (38.1%)
Suspicious	8/21 (38.1%)
Yes	5/21 (23.8%)
Vascular encasement	
No	5/21 (23.8%)
Hilar encasement	12/21 (57.1%)
Superior vena cava syndrome	5/21 (23.8%)
Other vessels' encasement	8/21 (38.1%)
2.c. Pleural component	
No	2/21 (9.6%)
Unilateral	17/21 (81%)
Bilateral	2/21 (9.6%)
Longest diameter (mm)	108 ± 47.8 (16–195)
Pleural effusion	10/21 (47.6%)

Longest diameters and SUVmax are given as mean ± standard deviation with range in parentheses. Results are number (no.) of patients/total number of patients with available information and percentage in parentheses

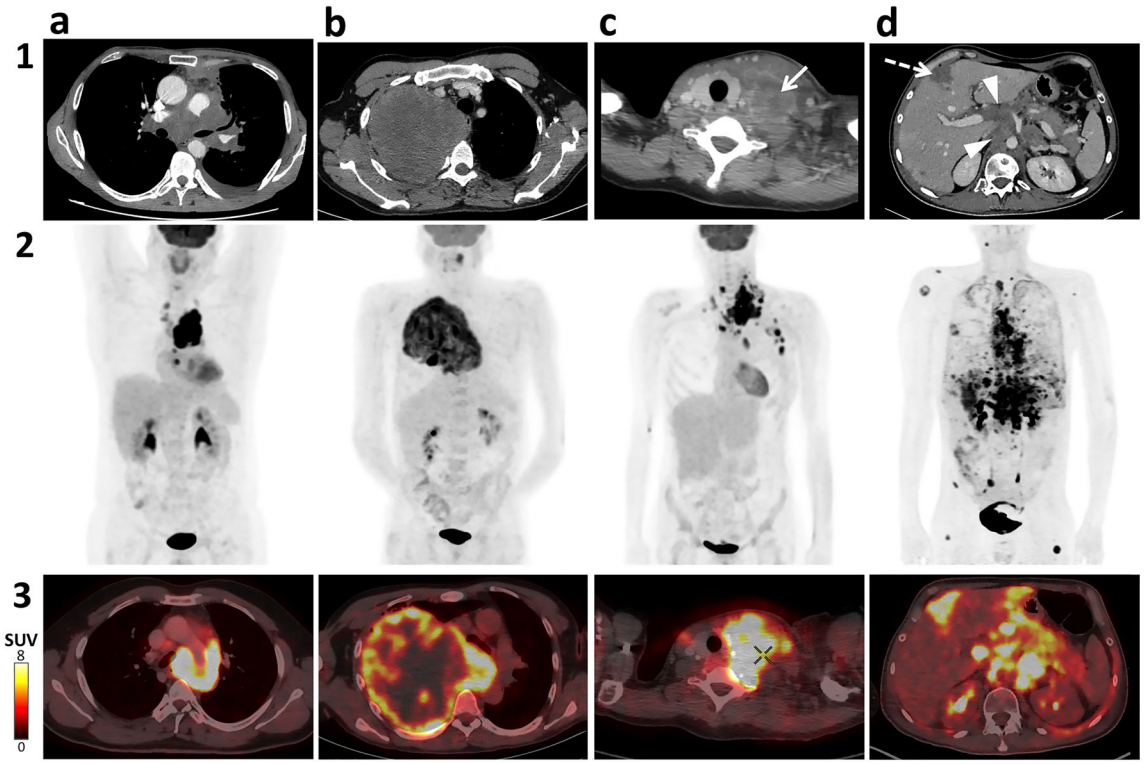

Fig. 1 Main radiological patterns of SMARCA4-deficient thoracic sarcomas. Four main radiological patterns, here in four different patients, were proposed: **a** mediastinal pattern, which consisted in an infiltrative mass of the middle and upper mediastinum with vascular, tracheal, esophagus, thymus, and bronchial invasions; **b** pleural pattern, which consisted in a large parietal and visceral heterogeneous mass with a pleural effusion, often unilateral; **c** cervical pattern, which consisted in multiple confluent ill-defined necrotic and large lymphadenopathies (white arrow); **d** retroperitoneal pattern, which consisted in a mainly retroperitoneal tumor infiltrate with encasements of the aorta, renal vessels, celiac artery, and portal vein (white arrowhead)—note the peritoneal sarcomatosis responsible for a scalloping at the anterior side of the liver (dashed arrow). Row 1 corresponds to axial chest CT scan after iodine-contrast agent injection and portal phase acquisition; row 2 corresponds to a coronal maximal intensity projection view of ^{18}F fluorodeoxyglucose position emission tomography (^{18}F-FDG-PET); row 3 corresponds to axial ^{18}F-FDG-PET merged with CT. Note the strong avidity of the lesions, whatever the main pattern and the tumor extension

heterogeneous aspect on post-contrast CT in all patients. Abnormal intra- and peritumoral vessels were seen once. Calcifications or cystic components were never seen.

When present, the mediastinal part of the tumor was often large (mean longest diameter 127.6 ± 56.6 mm (range 46–266)) and typically involved the upper and middle mediastinum unilaterally with an extension to the lung apex. Anteriorly, the thymic area was invaded in almost half of the patients. Posteriorly, the esophagus was at least circumferentially encircled in 13 patients of whom 5 showed an objective invasion of the mucosa. Vascular encasement was observed in 16 patients (76.2%) and consisted in unilateral encasement of hilar vessels in 12 patients (57.1%) but also of the superior vena cava, subclavian vessels, and innominate or internal jugular vein. The same ability to encircle vessels was seen for the patients with abdominal main tumor burden. The tumor was responsible for post-obstructive atelectasis in 11 patients.

A pleural solid component was present in 19 patients (90.4%), almost always unilateral when present, together with a pleural effusion in 10 patients (47.6%). The pleural main pattern could demonstrate different aspects (Fig. 2), from multiple ill-defined unilateral heterogeneous masses attached to parietal and visceral pleura with a pleural effusion to a large compressive heterogeneous unique mass that filled the whole thorax and crossed the intercostal muscles in order to spread among the soft tissue of the trunk wall.

When ^{18}F-FDG-PET/CT was available, the tumor and its metastases always demonstrated a strong ^{18}F-FDG avidity with a mean SUVmax of 16.6 ± 8.2 (range 9.1–33.8).

Table 3 summarizes the regional and distant extensions. Almost all patients showed lymphadenopathies involving more than 2 lymph node areas, most often spreading from mediastinal areas to the neck, along subclavian vessels up to the axillary area. In the abdomen, lymphadenopathies were mostly located in the celiac and retroperitoneal nodes above the kidneys. These lymphadenopathies showed central necrosis in 17 patients (81%), and the fat surrounding lymphadenopathies was clearly infiltrated in 13 patients (Fig. 3).

Eleven patients showed metastases at diagnosis. In descending order, metastases were located in one adrenal for 7

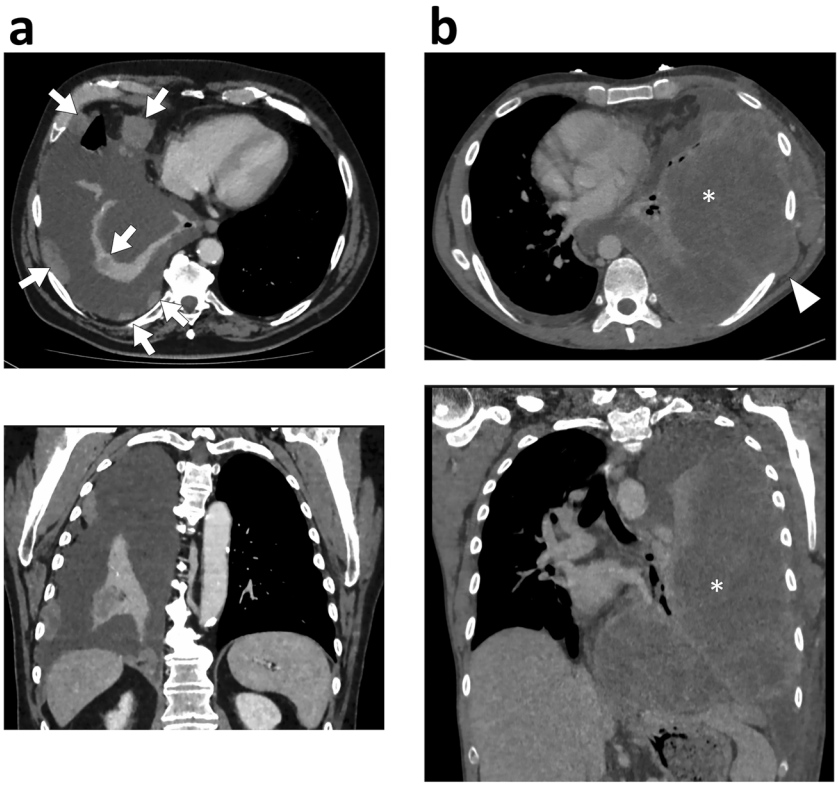

Fig. 2 Different aspects of the pleural main pattern of *SMARCA4*-deficient thoracic sarcomas. **a** A 72-year-old male presented with dyspnea and chest pain. CT scan after contrast agent injection showed multiple unilateral pleural masses from 1- to 6-cm longest axis with an abundant right pleural effusion and lung atelectasis. **b** A 31-year-old male presented with dyspnea, chest pain, and increased volume of the left hemi-thorax. CT scan after contrast agent injection showed a huge circumferential pleural mass with heterogeneous densities (white asterisk) that compressed the mediastinum and crossed the parietal pleura and the intercostal muscles to spread within soft tissue of the left thoracic wall (white arrowhead). Both patients had a history of smoking history (15 and 17 pack-years, respectively), but quit for more than 1 year before the beginning of the symptoms

patients, bilaterally in three cases; in the lung for six patients; in the bone for five patients—always lytic—with an epidural contiguous extension in two patients (Fig. 4); and in the brain for two patients. Three patients demonstrated an intra- or retroperitoneal sarcomatosis, located in the fat surrounding the kidney in 2 cases.

Interestingly, lung emphysema was present on the chest CT of 11 patients (52.4%). TNM classification for lung cancer staging, when applicable, is given in Supplemental Table 2: the staging group was at best stage IIIc.

Considering these initial clinical and radiological presentations, the first hypothesis according to medical records was a lymphoma (12 patients, 57.1%), a NMC (five patients, 23.8%), a malignant non-seminomatous germ cell tumor (MNSGCT) (two patients, 9.5%), or a lung carcinoma (two patients, 9.5%).

Pathological findings

Pathological samples came from biopsies in all cases. Pathologists reported the presence of large, poorly differentiated cells arranged in poorly cohesive sheets with an area of necrosis. Initial histopathological diagnosis included epithelioid sarcoma (eight patients), Ewing sarcoma (four patients), SMARCA4-DTS (3 patients), undifferentiated thymic carcinoma (two patients), undifferentiated malignant neoplasm (two patients), MRT (one patient), and undifferentiated carcinoma (one patient).

Table 4 summarizes the immunohistochemistry analyses. All tumors lost the (gene) expression of SMARCA4 (BRG1). There was a positive immunostaining for SOX2 in 17 out of 19 patients (89.5%) and for CD34 in 16 out of 21 patients (76.2%). When performed, markers for NMC, thymus cancer, and lung adenocarcinoma were always negative. Epithelial markers were positive in 10 out of 16 cases (including 6 focal positivity). Synaptophysin was focally positive in three samples. Somatic mutations of SMARCA4 were found in all cases when mutational analysis by RNAseq was performed. Figure 5 shows the typical pathological and molecular findings in a patient with SMARCA4-DTS.

Table 3 Imaging features of the regional and distant extensions of *SMARCA4*-deficient thoracic sarcomas

Characteristics	No. of patients (%)
3.a. Lymph node metastases	
Number of metastatic lymph nodes	
0	2/21 (9.5%)
1	0/21 (0%)
2–5	10/21 (47.6%)
> 5	9/21 (42.9%)
Necrotic lymphadenopathy	19/21 (90.5%)
Ill-defined lymphadenopathy	13/21 (61.9%)
Lymph node areas involved by SMARCA4-DTS	
Mediastinal[1]	19/21 (90.5%)
Internal thoracic	15/21 (71.4%)
Cervical-subclavian[2]	13/21 (61.9%)
Abdominal (intra- or retroperitoneal)	6/21 (28.6%)
Axillary	5/21 (23.8%)
3.b. Other metastases	
Adrenal	10/21 (47.6%)
Lung	6/21 (28.6%)
Bone	5/21 (23.8%)
Intra- or retroperitoneal sarcomatosis	3/16 (18.8%)
Liver	2/16 (12.5%)
Epidural	2/21 (9.6%)
Brain	2/21 (9.6%)

Results are number (no.) of patients/total number of patients with available information and percentage in parentheses

[1] Mediastinal locations correspond to lymphadenopathies in the following lymph node of the International Association for the Study of Lung Cancer (IASLC) map: 2R/L, 3R/L, 4R/L, 5R/L, 6R/L, 7R/L, 8 R/L, 9R/L, 10R/L, and/or 11R/L

[2] Cervical-subclavian locations correspond to lymphadenopathies in the following 1R/L lymph node of the IASCL map and/or located in any other lymph node of the cervix

Outcome

First-line chemotherapy regimen consisted in anthracycline-based chemotherapy in nine patients and platinum salts in eight patients. Two had a curative surgery (pneumonectomy) followed by radiotherapy. Early relapse or progression constantly occurred. Finally, all the patients died of their disease due to local complications, with a median survival of 5 months after diagnosis (range 1–13). The radiological follow-up of a patient is illustrated in Fig. 6, showing the aggressive course of the disease.

Discussion

Our results shows that although SMARCA4-DTS do not have perfectly specific radiological features, the coexistence of heterogeneous ill-defined mass with both compressive and infiltrative invasions of adjacent organs and multiple prominent necrotic and ill-defined lymphadenopathies integrated with the clinical setting should raise radiological suspicion for this rare tumor.

Though these tumors are rare, they are above all exceedingly aggressive. SMARCA4-DTS should be considered an oncologic emergency since at least eight of the patients from our series presented with life-threatening initial symptoms (e.g., high digestive hemorrhage, hemoptysis, and superior vena cava syndrome). Thus, we believe that radiologists must be aware of this entity because the hypothesis of a SMARCA4-DTS may orient the differential diagnosis and lead to additional immunohistochemistry that is not often routinely prescribed for lung tumors—SOX2, CD34, and BRG1 immunostaining—therefore avoid diagnostic wandering.

Our findings concur with the literature. Smoking history and male predominance were also found by Le Loarer et al, Yoshida et al, and Sauter et al [1, 5, 6]. Median age was 41, 39, and 59 years old in these three studies.

These other studies also distinguished different locations of the main tumor burden: mainly mediastinum, lung, and pleura. Interestingly, Yoshida et al found one tumor that involved the axillary area and spared the thoracic cavity and three cases with simultaneous large masses of the thoracic and abdominal cavities at diagnosis, making it difficult to identify the initial location [5]. Herein, the main tumor burden of one patient was located in the retroperitoneum but he also showed several thoracic lymphadenopathies. Thus, SMARCA4-DTS cannot be restricted to a pattern-based approach and additional features are required. We have deepened the previous studies by identifying a high prevalence of ill-defined tumors with heterogeneous densities compatible with necrosis, with no noticeable abnormal vascularization, no calcification, and no cystic changes. The striking feature was the ability of these tumors to cross compartments and to spread from mediastinum to pleura, neck, or lung apex in an infiltrative and compressive way. Hence, all patients died of local complications and not of metastasis. We found extreme cases illustrating these abilities: huge pleural tumor crossing the intercostal muscles of an infiltrative tumor of the posterior mediastinum spreading to epidural spaces and vertebral body.

Le Loarer et al highlighted the presence of lymphadenopathies at diagnosis, but our results deepened this depiction and stressed the high prevalence of confluent, necrotic, and ill-defined lymphadenopathies with surrounding infiltrate at diagnosis [1]. Since lymphoma was frequently suspected, one could oppose the morphology of the lymphadenopathies in these two diseases, lymph node metastases in lymphoma being better limited, more homogeneous, and round. Our study also highlights a tropism for lymphatic spreading, which is a rare feature for sarcomas and could help establishing diagnostic hypotheses.

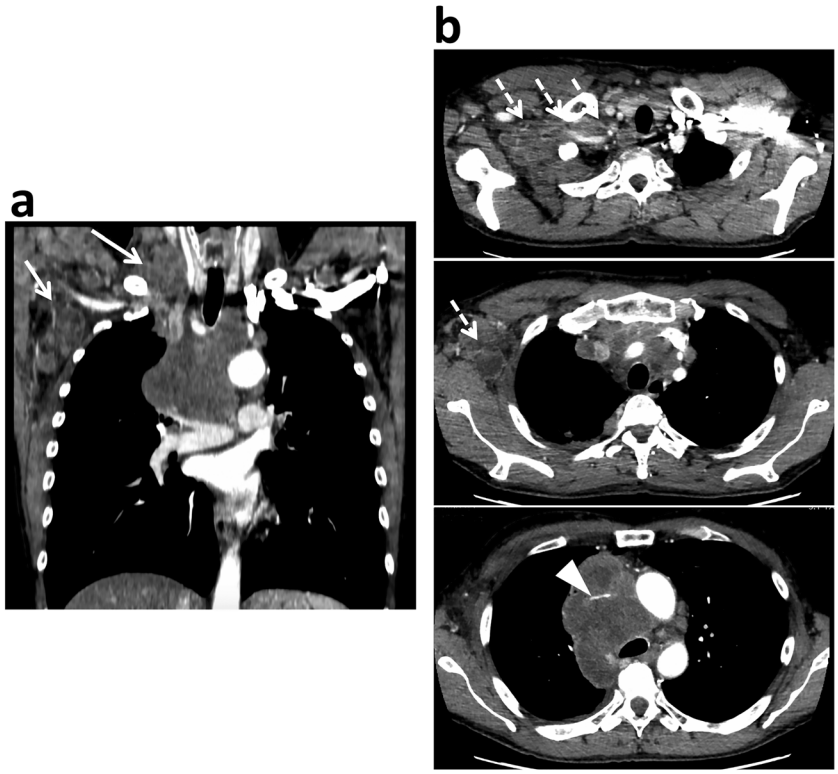

Fig. 3 Lymphatic tropism of *SMARCA4*-deficient thoracic sarcomas. A 54-year-old male with a 30-pack-year smoking history presented with dyspnea and superior vena cava syndrome. A chest computed tomography with iodine-contrast agent injection was performed with (**a**) coronal and (**b**) axial reformations. One can note the multiple lymphadenopathies involving the left lower jugular-carotid, subclavian, and axillary lymph node areas (white arrows), as well as the central necrosis in all of them. These lymphadenopathies tended to merge and demonstrated ill-defined margins with discrete fatty infiltration around them. The mediastinal main tumor burden was located in the upper mediastinum, asymmetrically on the right, with superior vena cava compression responsible for the symptoms (white arrowhead)

Besides lymph node metastases, 11 patients from our series showed distant metastases at presentation in the adrenal, lung, bone (with contiguous epiduritis), liver, and brain, which is consistent with the literature. Yoshida et al also reported the case of an ovarian metachronous metastasis. All the patients of these studies died of disease within 13 months except for four patients in the study by Yoshida et al (with less than 7 months of follow-up) [1, 5, 6].

The radiological differential diagnoses depend on the main radiological pattern. A mediastinal pattern can suggest thymic carcinoma, lymphoma, MNSGCT, and small cell lung carcinoma (SCLC). Contrary to SMARCA4-DTS, the epicenter of thymic carcinoma is always the anterior mediastinum; they can show cystic changes and calcifications and be revealed by paraneoplastic syndrome [15, 16]. Unlike SMARCA4-DTS, SCLC affects older patients from 60 to 70 years old and calcifications may be seen in 23% of patients [17–19]. MNSGCT is mostly found in the anterosuperior mediastinum of young adults from 20 to 40 years old. Though no imaging features seem discriminant, these tumors secrete α-fetoprotein and β-human chorionic gonadotropin [20, 21]. A pleural pattern could suggest malignant solitary fibrous tumor (SFT) and malignant pleural mesothelioma. Unlike SMARCA4-DTS, SFT typically demonstrates large intra- and peritumoral vessels, no ill-defined necrotic lymphadenopathies, and lower SUVmax [22–24]. Finally, primary pulmonary NMC share several characteristics with SMARCA4-DTS as they occur in young adults, can asymmetrically involve the pleura, mediastinum, and lymph nodes, and demonstrate intense ^{18}F-FDG avidity [7–9]. Both tumor types are very clinically aggressive.

Herein, the 8 tumors and their metastases imaged by ^{18}F-FDG-PET/CT demonstrated a strong metabolic activity. The lowest SUVmax of our series was 9. Hence, this imaging modality could be used for staging, guidance of needle core biopsies, and response evaluation. However, it cannot be used to discriminate between other histotypes because SCLC, NSCLC, thymic carcinoma, lymphoma, and MNSGCT can also demonstrate high metabolic activity [25–27].

Interestingly, SMARCA4-DTS are molecularly close to MRT and small cell carcinoma of the ovary—hypercalcemic type, all showing an inactivation of the SMARCA4 gene [1]. These hypotheses are different from the radiological ones, and to our knowledge, a primary location in the chest cavity has

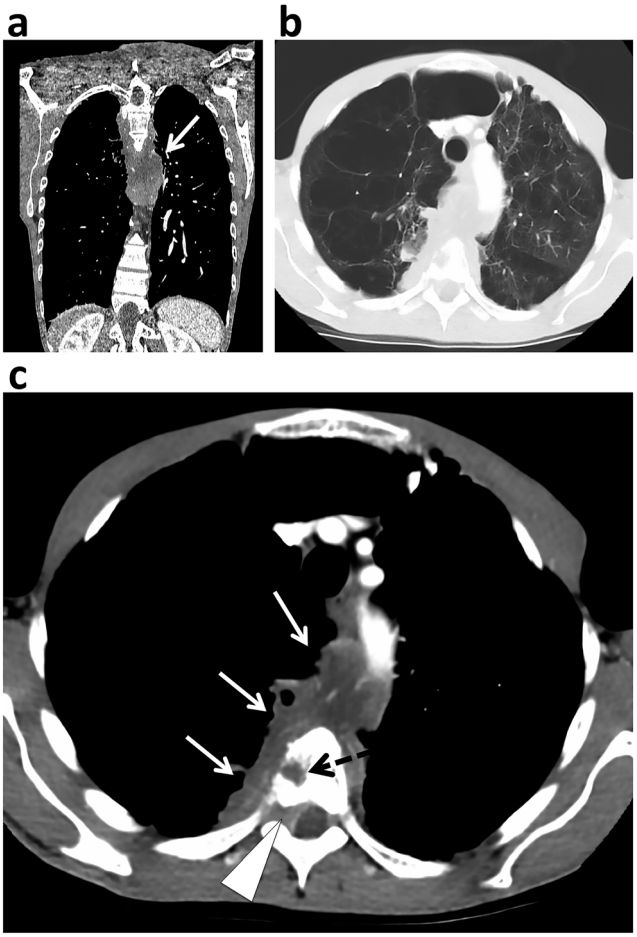

Fig. 4 Infiltration and invasion of adjacent organs by *SMARCA4*-deficient thoracic sarcomas. A 41-year-old male with a 50-pack-year smoking history and lung emphysema presented with a rapidly progressing chest pain. A chest computed tomography with iodine-contrast agent injection was performed with coronal (**a**) and axial reformations including lung (**b**) and mediastinal windowing (**c**). The main tumor burden was located in the posterior and upper mediastinum (white arrow) and spread posteriorly on each side of the vertebral body, infiltrated the D4-D5 right intervertebral foramen, and was responsible for a lateral epiduritis (white arrowhead). One can note the bone metastasis (black dashed arrow), likely in contiguity with the main tumor

Table 4 Pathological and molecular findings in *SMARCA4*-deficient thoracic sarcomas

Characteristics	No. of patients (%)
Histological initial diagnosis	
US—rhabdoid	1/21 (4.8%)
US—round cell	4/21 (19%)
US—epithelioid	8/21 (38.1%)
Undifferentiated thymic carcinoma	2/21 (9.5%)
Undifferentiated carcinoma	1/21 (4.8%)
Undifferentiated malignant neoplasm	2/21 (9.5%)
SMARCA4-DTS	3/21 (14.3%)
Immunohistochemistry	
Surrogate markers of SMARCA4-DTS	
BRG1 staining: loss	21/21 (100%)
SOX2 staining: positive	17/19 (89.5%)
CD34 staining: positive	16/21 (76.2%)
Differential diagnoses	
Cytokeratins (AE1/AE3)	
Negative	6/16 (37.5%)
Focal staining	6/16 (37.5%)
Diffuse staining	4/16 (25%)
Thymic markers (CD5/CD117)	
Negative	16/16 (100%)
Squamous markers (p40/p63)	
Negative	14/14 (100%)
Lung adenocarcinoma marker (TTF-1)	
Negative	18/18 (100%)
NUT midline carcinoma marker (NUT)	
Negative	11/11 (100%)
Neuroendocrine markers (chromogranin A/synaptophysin)	
Both negative	8/11 (72.7%)
Isolated synaptophysin: focal staining	1/11 (9.1%)
Isolated synaptophysin: diffuse staining	2/11 (18.2%)

Results are number (no.) of patients/total number of patients with available information and percentage in parentheses

US undifferentiated sarcoma, *SMARCA4-DTS SMARCA4*-deficient thoracic sarcoma

not been described for these other entities. Therefore, radio-pathological correlations could help restrict complementary immunohistochemistry and molecular analyses [28, 29].

Our study has limits. This is a retrospective study, but this seems unavoidable given the rarity and recent description of these tumors. Second, the imaging protocol was not standardized with differences in the acquisition of parameters. Third, the lymph node and distant metastases were not confirmed by the pathological analysis of biopsy samples. For patients without a baseline ^{18}F-FDG-PET/CT, this could have led to ill estimation of the exact metastatic extension. Moreover, a case-control study could have identified radiological features to distinguish SMARCA4-DTS from other tumors. However, building a representative and exhaustive control cohort would have been difficult. Some of the main differential diagnoses for pathologists (i.e., NMC, MNSGCT, thymic carcinomas, other intra-thoracic sarcomas …) are also very rare with a strong risk of selection bias. Giving the heterogeneity in clinical and radiological presentations and the limited size of our study population, further cases are required to validate our findings and to confirm our radiological depictions of SMARCA4-DTS. Actually, our aim was to provide a first report of these rare tumors dedicated to radiologists so they could be able to raise the hypothesis of SMARCA4-DTS when appropriate, to guide the histological and molecular analyses after the biopsy because those for SMARCA4-DTS

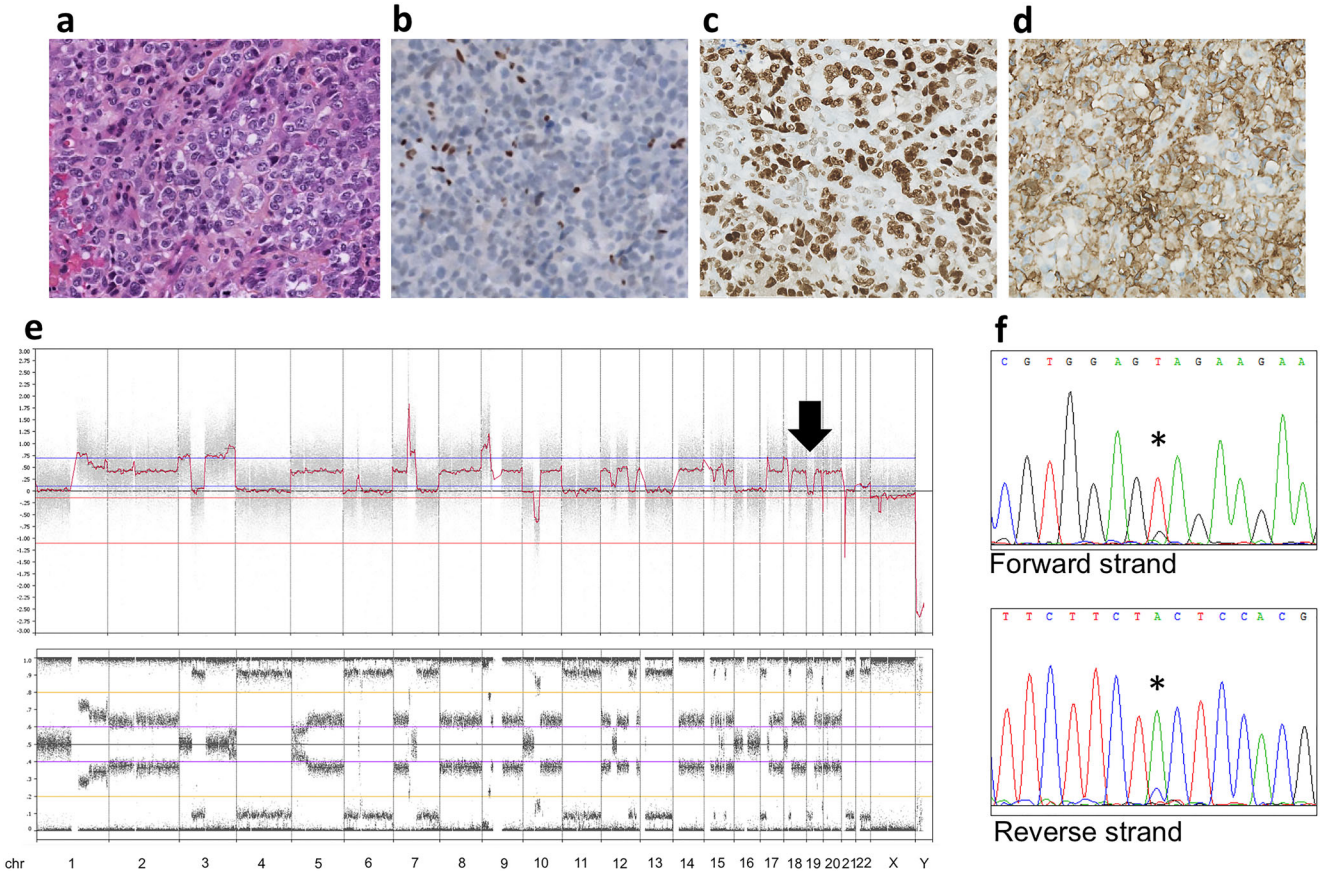

Fig. 5 Typical histological and molecular findings of *SMARCA4*-deficient thoracic sarcomas. **a** Hematoxylin- and eosin-stained slices of the biopsy sample showed tumor cells that were arranged in poorly cohesive sheets. A diagnosis of unclassified sarcoma with epithelioid phenotype was initially rendered. **b** SMARCA4/BRG1 immunostaining shows a loss of SMARCA4 nuclear expression in tumor cells in contrast with normally stained inflammatory and endothelial cells. **c** Tumor cells stain diffusely for SOX2 and (**d**) heterogeneously for CD34. **e** Genomic profiling of the tumor indicates a complex profile with loss of heterozygosity on 19p encompassing *SMARCA4* locus (black arrow). **f** Sanger sequencing on tumor DNA highlights an exon14:c.G2056T missense mutation of *SMARCA4* indicated with asterisk on forward and reverse strands

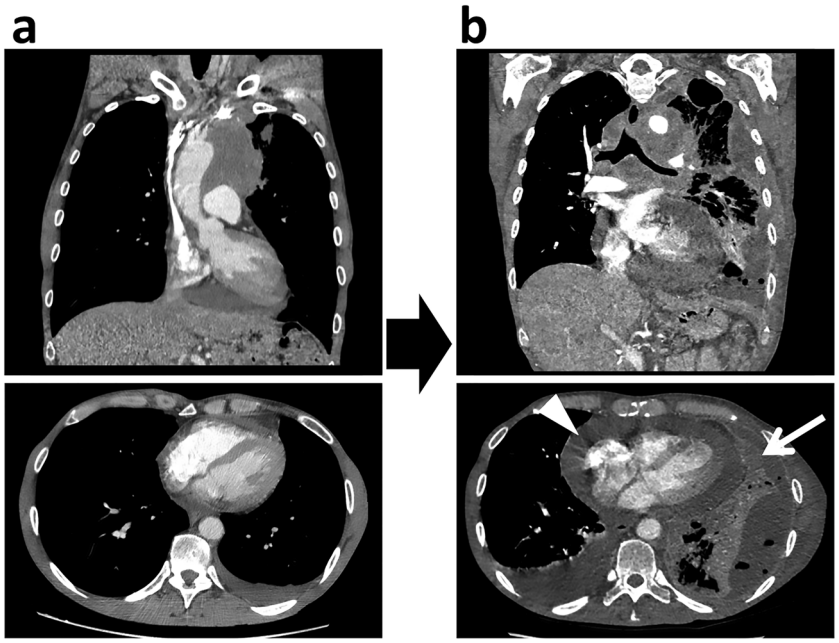

Fig. 6 Rapid progression of *SMARCA4*-deficient thoracic sarcoma in a 39-year-old male. On baseline chest computed tomography (**a**), the tumor was mainly located in the right upper mediastinum with small pericardial and left pleural effusions. The patient was treated with chemotherapy based on cisplatin and Taxol. The next evaluation (**b**) 2 months later showed that the disease was progressing strongly with multiple new pleural lesions (white arrow), new mediastinal lymphadenopathies encircling the trachea and the two holes, and unequivocal increase of the pleural and pericardial effusions (white arrowhead)

are not routinely performed, and to help during radiopathological correlations. Furthermore, although exhaustive, none of our conventional radiological features would be perfectly specific and discriminant to diagnose SMARCA4-DTS. Finally, none of the patients underwent a chest MRI although it could have provided additional features to characterize the signal, architecture, margins, and vascularization of SMARCA4-DTS and may have helped identify more specific features of these tumors [30].

To conclude, SMARCA4-DTS is a rare undifferentiated sarcoma with a very aggressive course and a poor short-term prognosis due to local evolution. Radiologists should evoke this entity when confronted to middle-aged patients, especially male smokers presenting with an ill-defined, heterogeneous, and large tumor of the chest cavity demonstrating several necrotic lymphadenopathies and both compressive and infiltrative abilities. Given its propensity to metastasize and its metabolic activity, staging should include a whole-body imaging, including brain imaging and ^{18}F-FDG-PET/CT.

Acknowledgements The authors would like to thank Ms. Camille Martinerie for medical writing services.

Funding The authors state that this work has not received any funding.

Compliance with ethical standards

Guarantor The scientific guarantor of this publication is Dr. Xavier Buy, MD, head of the Department of Radiology, Institut Bergonié, Bordeaux, France.

Conflict of interest The authors of this manuscript declare no relationships with any companies, whose products or services may be related to the subject matter of the article.

Statistics and biometry No complex statistical methods were necessary for this paper.

Informed consent Written informed consent was waived by the Institutional Review Board.

Ethical approval Institutional Review Board approval was obtained.

Study subjects or cohorts overlap Some study subjects or cohorts have been previously reported in the study by Le Loarer et al which aim was to characterize the molecular and genetic aspects of SMARCA4-DTS and did include a dedicated radiological analysis (Nat Genet 47(2015):1200–1205).

Methodology
- retrospective
- observational
- multi-center study

References

1. Le Loarer F, Watson S, Pierron G et al (2015) SMARCA4 inactivation defines a group of undifferentiated thoracic malignancies transcriptionally related to BAF-deficient sarcomas. Nat Genet 47:1200–1205. https://doi.org/10.1038/ng.3399
2. Wong AK, Shanahan F, Chen Y et al (2000) BRG1, a component of the SWI-SNF complex, is mutated in multiple human tumor cell lines. Cancer Res 60:6171–6177
3. Wilson BG, Roberts CW (2011) SWI/SNF nucleosome remodellers and cancer. Nat Rev Cancer 11:481–492. https://doi.org/10.1038/nrc3068
4. Kadoch C, Hargreaves DC, Hodges C et al (2013) Proteomic and bioinformatic analysis of mammalian SWI/SNF complexes identifies extensive roles in human malignancy. Nat Genet 45:592–601. https://doi.org/10.1038/ng.2628
5. Yoshida A, Kobayashi E, Kubo T et al (2017) Clinicopathological and molecular characterization of SMARCA4-deficient thoracic sarcomas with comparison to potentially related entities. Mod Pathol 30:797–809. https://doi.org/10.1038/modpathol.2017.11
6. Sauter JL, Graham RP, Larsen BT, Jenkins SM, Roden AC, Boland JM (2017) SMARCA4-deficient thoracic sarcoma: a distinctive clinicopathological entity with undifferentiated rhabdoid morphology and aggressive behavior. Mod Pathol 30:1422–1432. https://doi.org/10.1038/modpathol.2017.61
7. Parikh SA, French CA, Costello BA et al (2013) NUT midline carcinoma: an aggressive intrathoracic neoplasm. J Thorac Oncol 8:1335–1338. https://doi.org/10.1097/JTO.0b013e3182a00f41
8. Travis WD, Brambilla E, Nicholson AG et al (2015) The 2015 World Health Organization classification of lung tumors: impact of genetic, clinical and radiologic advances since the 2004 classification. J Thorac Oncol 10:1243–1260. https://doi.org/10.1097/JTO.0000000000000630
9. Sholl LM, Nishino M, Pokharel S et al (2015) Primary pulmonary NUT midline carcinoma: clinical, radiographic, and pathologic characterizations. J Thorac Oncol 10:951–959. https://doi.org/10.1097/JTO.0000000000000545
10. Kuwamoto S, Matsushita M, Takeda K et al (2017) SMARCA4-deficient thoracic sarcoma: report of a case and insights into how to reach the diagnosis using limited samples and resources. Hum Pathol 70:92–97. https://doi.org/10.1016/j.humpath.2017.05.024
11. Chan-Penebre E, Armstrong K, Drew A et al (2017) Selective killing of SMARCA2- and SMARCA4-deficient small cell carcinoma of the ovary, hypercalcemic type cells by inhibition of EZH2: in vitro and in vivo preclinical models. Mol Cancer Ther 16:850–860. https://doi.org/10.1158/1535-7163.MCT-16-0678
12. Yamagishi M, Uchimaru K (2017) Targeting EZH2 in cancer therapy. Curr Opin Oncol 29:375–381. https://doi.org/10.1097/CCO.0000000000000390
13. Italiano A, Soria JC, Toulmonde M et al (2018) Tazemetostat, an EZH2 inhibitor, in relapsed or refractory B-cell non-Hodgkin lymphoma and advanced solid tumours: a first-in-human, open-label, phase 1 study. Lancet Oncol 19:649–659. https://doi.org/10.1016/S1470-2045(18)30145-1
14. Young H, Baum R, Cremerius U et al (1999) Measurement of clinical and subclinical tumour response using [18F]-fluorodeoxyglucose and positron emission tomography: review and 1999 EORTC recommendations. European Organization for Research and Treatment of Cancer (EORTC) PET Study Group. Eur J Cancer 35:1773–1782
15. Rosado-de-Christenson ML, Strollo DC, Marom EM (2008) Imaging of thymic epithelial neoplasms. Hematol Oncol Clin North Am 22:409–431. https://doi.org/10.1016/j.hoc.2008.03.011

16. Jung KJ, Lee KS, Han J, Kim J, Kim TS, Kim EA (2001) Malignant thymic epithelial tumors: CT-pathologic correlation. AJR Am J Roentgenol 176:433–439. https://doi.org/10.2214/ajr.176.2.1760433
17. Carter BW, Glisson BS, Truong MT, Erasmus JJ (2014) Small cell lung carcinoma: staging, imaging, and treatment considerations. Radiographics 34:1707–1721. https://doi.org/10.1148/rg.346140178
18. Kurihara Y, Nakajima Y, Ishikawa T (1993) The prevalence and pattern of calcification in primary lung carcinoma as demonstrated by computed tomography [in Japanese]. Hai Gan 1993 33(7):1037–1044. https://doi.org/10.2482/haigan.33.1037
19. Grewal RG, Austin JH (1994) CT demonstration of calcification in carcinoma of the lung. J Comput Assist Tomogr 18:867–871
20. Drevelegas A, Palladas P, Scordalaki A (2001) Mediastinal germ cell tumors: a radiologic-pathologic review. Eur Radiol 11:1925–1932. https://doi.org/10.1007/s003300000725
21. Ueno T, Tanaka YO, Nagata M et al (2004) Spectrum of germ cell tumors: from head to toe. Radiographics 24:387–404. https://doi.org/10.1148/rg.242035082
22. Yeom YK, Kim MY, Lee HJ, Kim SS (2015) Solitary fibrous tumors of the pleura of the thorax: CT and FDG PET characteristics in a tertiary referral center. Medicine (Baltimore) 94:e1548. https://doi.org/10.1097/MD.0000000000001548
23. Chick JFB, Chauhan NR, Madan R (2013) Solitary fibrous tumors of the thorax: nomenclature, epidemiology, radiologic and pathologic findings, differential diagnoses, and management. AJR Am J Roentgenol 200:W238–W248. https://doi.org/10.2214/AJR.11.8430
24. Ginat DT, Bokhari A, Bhatt S, Dogra V (2011) Imaging features of solitary fibrous tumors. AJR Am J Roentgenol 196:487–495. https://doi.org/10.2214/AJR.10.4948
25. Vilstrup MH, Torigian DA (2014) [18F] Fluorodeoxyglucose PET in thoracic malignancies. PET Clin 9:391–420, v. https://doi.org/10.1016/j.cpet.2014.06.002
26. Quint LE (2006) PET: other thoracic malignancies. Cancer Imaging 6:S82–S88. https://doi.org/10.1102/1470-7330.2006.9015
27. Treglia G, Sadeghi R, Annunziata S et al (2014) Diagnostic accuracy of 18F-FDG-PET and PET/CT in the differential diagnosis between malignant and benign pleural lesions: a systematic review and meta-analysis. Acad Radiol 21:11–20. https://doi.org/10.1016/j.acra.2013.09.015
28. Wu WW, Bi WL, Kang YJ et al (2016) Adult atypical teratoid/rhabdoid tumors. World Neurosurg 85:197–204. https://doi.org/10.1016/j.wneu.2015.08.076
29. Korivi BR, Javadi S, Faria S et al (2017) Small cell carcinoma of the ovary, hypercalcemic type: clinical and imaging review. Curr Probl Diagn Radiol. https://doi.org/10.1067/j.cpradiol.2017.08.004
30. Takahashi K, Al-Janabi NJ (2010) Computed tomography and magnetic resonance imaging of mediastinal tumors. J Magn Reson Imaging 32:1325–1339. https://doi.org/10.1002/jmri.22377